Hindawi
Advances in Mathematical Physics
Volume 2023, Article ID 2729561, 16 pages
https://doi.org/10.1155/2023/2729561

Research Article

Effect of Classical and Quantum Superposition of Atomic States on Quantum Correlations

Chimdessa Gashu,[1,2,3] **Ebisa Mosisa**,[1] **and Chali Idosa**[1]

[1]*Department of Physics, Jimma University, P.O. Box. 378, Jimma, Ethiopia*
[2]*Institute of Atomic and Molecular Sciences, Taiwan International Graduate Program, Taipei 10617, Taiwan*
[3]*Department of Physics, National Central University, P.O. Box. 320317, Taipei 10617, Taiwan*

Correspondence should be addressed to Ebisa Mosisa; ebmosisa@gmail.com

Received 27 October 2022; Revised 1 April 2023; Accepted 8 April 2023; Published 11 May 2023

Academic Editor: Laurent Raymond

In this paper, we report the effect of classical and quantum superposition of atomic states on quantum correlations. Coupled photon pairs generated in a ladder quantum beat laser using coherent-induced classical field and atomic state coherent superposition are considered. Once the quantum coherence get sufficient time, it can generate quantum correlations that include quantum discord, quantum entanglement, and quantum steering, which quickly increase with time until they get their maximum strength. Their strength can be improved further by increasing the number of superposed atoms per unit time, selecting an appropriate amplitude of the classical fields, and managing the amount of temperatures and phase fluctuations. In particular, two-way quantum steering, which is a guarantee for the existence of quantum discord and quantum entanglement, can be achieved by increasing the rate of atomic injection from 2 kHz to 25 kHz even if the mean temperature of the heat bath is considered. The maximum achievable strength of quantum correlations is enhanced by increasing the rate of atomic injection and choosing an appropriate parameters of the coherent-induced classical field in the open quantum system which is treated by using the density operator approach.

1. Introduction

Quantum correlations have been the subject of intensive studies in the past two decades, mainly due to the general belief that they are a fundamental resource for quantum information processing tasks. The first rigorous attempt to address the classification of quantum correlation has been put forward by Werner [1], who put on a firm basis on the elusive concept of quantum entanglement. Quantum superpositions are quantum mechanical principles that are at the heart of quantum information and communication applications [2]. In addition, quantum superposition, which is often called quantum coherence of two states, plays a fundamental role in quantum information and communication protocols. Quantum coherence is a local and nonclassical correlation of two or more quantum states [3, 4]. Quantum coherence is responsible for quantum features such as quantum discord, quantum entanglement, and quantum steering. Quantum features produced by the interaction of atoms and photons are powerful and suitable for quantum information and communication due to the relevant physical mechanisms and sources of decoherences that can be understood and easily modeled [5–8]. In particular, quantum features generated from strongly coupled photon pairs have been a long-sought goal in quantum information and communication in view of the fact that photons combine at high speed with long coherence times at room temperature [9]. To this aim, the modelling scheme that would generate strongly coupled photon pairs has becomes a great topic of interest among the current quantum information and communication researches [10, 11]. Generating and maintaining a strong quantum coherence between quantum particles, especially in the presence of decoherence, is one of the central goals of quantum information and communication protocols [12]. To this effect, researches have been conducted to study the role of thermal light on quantum entanglement generated by a cascaded

quantum beat laser, and the mean photon number of thermal light appears to degrade the entanglement [13]. Ullah et al. have studied quantum features in two-photon correlated spontaneous emission lasers [14]. They have proved that a correlated spontaneous emission laser is an active quantum system with invaluable applications in quantum information processing. Originally, quantum beat lasers were used for lasing without population inversion and quenching of spontaneous emission noise [15]. Recent studies show that quantum beat laser systems are a suitable source of quantum squeezing and quantum entanglement in which the quantum coherence is induced by driven fields [16, 17]. These quantum features may suggest the existence of other quantum features such as quantum discord and quantum steering, although they are not investigated so far. When correlated quantum states are used as a resource for teleportation, teleportation fidelity reveals two different aspects of nonclassicality or measures of correlations of quantum nature. The quantum correlations between the output two-mode Gaussian state of the cavity field depend on the Rabi frequency of the coupling fields and on the cavity damping rates. Specifically, the time evolution of quantum discord and entanglement become independent (dependent) of the purity (nonclassicality) of the initial states of the cavity field. Nonetheless, both the nonclassicality and purity, in the latter case, influence the quantum steering and nonlocality. Consequently, quantum nonlocality leads steerability, and quantum steering shows entanglement in the correlated field of the laser cavity. The reverse, however, does not exhibit always [18].

The main objective of these article is to study the effects of classical and quantum superposition of atomic states on quantum steering, entanglement, and discord by applying the master equation approach when the quantum coherences built up between photon pairs in a ladder quantum beat laser subjected to quantum decoherences originated by phase fluctuation and temperature of heat bath.

2. The Model and Dynamics of the System

We consider a three-level atomic system in cascade configuration with energy levels $|a\rangle$, $|b\rangle$, and $|c\rangle$ which is placed inside a doubly resonant cavity as shown in Figure 1. Initially, the atom is prepared in coherent superposition of the ground state $|a\rangle$ and the upper excited state $|c\rangle$. The two modes $\hat{o}_1$ and $\hat{o}_2$ to be at resonance with the two transitions $|c\rangle \longrightarrow |b\rangle$ and $|b\rangle \longrightarrow |a\rangle$ are dipole allowed and direct transition between level $|c\rangle$ and level $|a\rangle$ to be dipole forbidden.

The quantum Hamiltonian expressions describing the interaction pictures of the quantum beat lasers have been derived using the rotating wave and electric dipole approximations and can be written as [19, 20]

$$\hat{H} = \hat{H}_1 + \hat{H}_2. \tag{1}$$

The interaction Hamiltonian of a quantum beat laser with the annihilation operators $\hat{o}_1$ and $\hat{o}_2$ and classical field

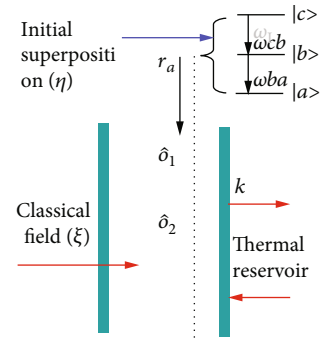

Figure 1: Schematic representation of atomic laser system coupled to reservoir, where r_a is the rate of atomic injection into the cavity and κ (kappa) is the cavity damping constant.

is expressed using the unitary operator $\hat{U} = \exp(-i\hat{H}_1 t)$, where $\hat{H}_1 = \sum_{u=a,b,c} \omega_u |u\rangle\langle u| + \omega_{ba}\hat{o}_1^\dagger \hat{o}_1 + \omega_{cb}\hat{o}_2^\dagger \hat{o}_2$ as

$$\begin{aligned}\hat{H}_2 = {} & ig\left[\hat{o}_1^\dagger |b\rangle\langle a| + \hat{o}_2^\dagger |c\rangle\langle b| - |a\rangle\langle b|\hat{o}_1 - |b\rangle\langle c|\hat{o}_2\right] \\ & + i\frac{\xi}{2}\left[|c\rangle\langle a| - |a\rangle\langle c|\right].\end{aligned} \tag{2}$$

With ξ being the classical field amplitude, here, we take the initial state of a single three-level atom considered:

$$|\psi(0)\rangle = C_a(0)|a\rangle + e^{-i\phi}C_c(0)|c\rangle, \tag{3}$$

where ϕ is is an arbitrary phase difference between the two states. The initial density operator for a single atom is expressible in the following form:

$$\rho(0) = \rho_{aa}^{(0)}|a\rangle\langle a| + \rho_{ac}^{(0)}e^{-\theta}|a\rangle\langle c| + \rho_{ca}^{(0)}e^{-\theta}|c\rangle\langle a| + \rho_{cc}^{(0)}|c\rangle\langle c|, \tag{4}$$

where θ represent the deviation of the phase fluctuation, $\rho_{aa}^{(0)} = |C_a(0)|^2$ and $\rho_{cc}^{(0)} = |C_c(0)|^2$ are the probability for the atom to be in the upper and lower levels at the initial time, and $\rho_{ac}^{(0)} = C_a(0)C_c^*(0)$ and $\rho_{ca}^{(0)} = C_c(0)C_a^*(0)$ represent the atomic state superposition at the initial time. We also note that $|\rho_{ac}^{(0)}|^2 = |\rho_{ca}^{(0)}|^2 = \rho_{aa}^{(0)}\rho_{cc}^{(0)}$. Considering the concept of the linear and adiabatic approximation schemes in the good cavity limit into account, we can find that the equation of evolution of the density operator for the cavity modes has the following form:

$$\begin{aligned}\frac{d}{dt}\hat{\rho}(t) = {} & \sum_1 \left[2\hat{o}_1^\dagger \hat{\rho}\hat{o}_1 - \hat{\rho}\hat{o}_1\hat{o}_1{}^\dagger - \hat{o}_1\hat{o}_1{}^\dagger\hat{\rho}\right] \\ & + \sum_2 \left[\left(2\hat{o}_2\hat{\rho}\hat{o}_2{}^\dagger - \hat{\rho}\hat{o}_2{}^\dagger\hat{o}_2 - \hat{o}_2{}^\dagger\hat{o}_2\hat{\rho}\right]\right. \\ & + \sum_3 \left[\hat{o}_1{}^\dagger\hat{\rho}\hat{o}_1 - \hat{\rho}\hat{o}_2{}^\dagger\hat{o}_1{}^\dagger + \hat{o}_2\hat{\rho}\hat{o}_1 - \hat{o}_1\hat{o}_2\hat{\rho}\right] \\ & + \sum_4 \left[\hat{o}_1{}^\dagger\hat{\rho}\hat{o}_2{}^\dagger - \hat{o}_2{}^\dagger\hat{o}_1{}^\dagger\hat{\rho} + \hat{o}_2\hat{\rho}\hat{o}_1 - \hat{\rho}\hat{o}_1\hat{o}_2\right],\end{aligned} \tag{5}$$

where

$$\Sigma_1 = \frac{A\left(\rho_{aa}^{(0)}\left(1+\left(\varepsilon^2/4\right)\right)-\rho_{ac}^{(0)}(3\varepsilon/2)+\rho_{cc}^{(0)}\left(3\varepsilon^2/4\right)\right)}{2(1+\varepsilon^2)(1+(\varepsilon^2/4))}, \quad (6)$$

$$\Sigma_2 = \frac{A\left(\rho_{aa}^{(0)}(3/4)\varepsilon^2+\rho_{ac}^{(0)}(3\varepsilon/2)+\rho_{cc}^{(0)}\left(1+\left(\varepsilon^2/4\right)\right)\right)}{2(1+\varepsilon^2)(1+(\varepsilon^2/4))}, \quad (7)$$

$$\Sigma_3 = \frac{A\left(-\rho_{aa}^{(0)}(\varepsilon/2)\left(1-\left(\varepsilon^2/2\right)\right)-\rho_{ac}^{(0)}\left(1-\left(\varepsilon^2/2\right)\right)+m_1\right)}{2(1+\varepsilon^2)(1+(\varepsilon^2/4))}, \quad (8)$$

$$\Sigma_4 = \frac{A\left(-\rho_{aa}^{(0)}\varepsilon\left(1+\left(\varepsilon^2/4\right)\right)-\rho_{ac}^{(0)}\left(1-\left(\varepsilon^2/2\right)\right)+m_2\right)}{2(1+\varepsilon^2)(1+(\varepsilon^2/4))}, \quad (9)$$

where $A = 2g^2 r_a/r^2$, $\varepsilon = \xi/\gamma$, $m_1 = \rho_{cc}^{(0)}\varepsilon(1+(\varepsilon^2/4))$, and $m_2 = \rho_{cc}^{(0)}(\varepsilon/2)(1-(\varepsilon^2/2))$.

On the other hand, the time evolution of the density operator for a two-mode cavity radiation coupled to a two-mode thermal reservoir via a single-port mirror is found as follows [21]:

$$\begin{aligned}\frac{d\widehat{\rho}}{dt} &= \frac{\kappa}{2}\left(\bar{N}_{th}+1\right)\left[2\widehat{o}_1\widehat{\rho}\widehat{o}_1^{\dagger}-\widehat{o}_1^{\dagger}\widehat{o}_1\widehat{\rho}-\widehat{\rho}\widehat{o}_1^{\dagger}\widehat{o}_1\right]\\ &+\frac{1}{2}\kappa\bar{N}_{th}\left[2\widehat{o}_2^{\dagger}\widehat{\rho}\widehat{o}_2-\widehat{o}_2\widehat{o}_2^{\dagger}\rho-\widehat{\rho}\widehat{o}_2\widehat{o}_2^{\dagger}\right]\\ &+\frac{1}{2}\left(2\Sigma_1+\kappa\bar{N}_{th}\right)\left[2\widehat{o}_1^{\dagger}\widehat{\rho}\widehat{o}_1-\widehat{o}_1\widehat{o}_1^{\dagger}\widehat{\rho}-\widehat{\rho}\widehat{o}_1\widehat{o}_1^{\dagger}\right]\\ &+\frac{1}{2}\left(2\Sigma_2+\kappa\left(\bar{N}_{th}+1\right)\right)\left[2\widehat{o}_2\widehat{\rho}\widehat{o}_2^{\dagger}-\widehat{o}_2^{\dagger}\widehat{o}_2\widehat{\rho}-\widehat{\rho}\widehat{o}_2^{\dagger}\widehat{o}_2\right]\\ &-\Sigma_3\left[\widehat{o}_1\widehat{o}_2\widehat{\rho}-\widehat{o}_1^{\dagger}\widehat{\rho}\widehat{o}_2^{\dagger}+\widehat{\rho}\widehat{o}_2^{\dagger}\widehat{o}_1^{\dagger}-\widehat{o}_2\widehat{\rho}\widehat{o}_1\right]\\ &-\Sigma_4\left[\widehat{o}_2^{\dagger}\widehat{o}_1^{\dagger}\widehat{\rho}-\widehat{o}_1^{\dagger}\widehat{\rho}\widehat{o}_2^{\dagger}+\widehat{\rho}\widehat{o}_1\widehat{o}_2-\widehat{o}_2\widehat{\rho}\widehat{o}_1\right].\end{aligned} \quad (10)$$

Equation (10) can be used to derive equations of motion for the expectation values of various system operators as a function of time. Considering Equations (6)-(9) and (10), we can write

$$\frac{d}{dt}o_1 = -\frac{\gamma_1}{2}o_1+\frac{\nu_1}{2}o_2^{*}+\widehat{o}_1^{(\mathrm{in})}, \quad (11)$$

$$\frac{d}{dt}o_2^{*} = -\frac{\gamma_2}{2}o_2^{*}-\frac{\nu_2}{2}o_1+\left(\widehat{o}_2^{(\mathrm{in})}\right)^{*}, \quad (12)$$

in which $\gamma_1 = \kappa - \Sigma_1$, $\nu_1 = \Sigma_2$, $\gamma_2 = \kappa + \Sigma_3$, and $\nu_2 = \Sigma_4$. Similarly, we can derive equation for expectation value of the remaining operators as Equations (A.2)-(A.8); $\widehat{o}_1^{(\mathrm{in})}(t)$ and $(\widehat{o}_2^{(\mathrm{in})})^{*}(t)$ are the noise forces whose correlation properties will be determined. Moreover, making use of Equations (11) and (12), it is possible to verify the expectation values of the time-dependent noise force as the following:

$$\left\langle \widehat{o}_1^{(\mathrm{in})}(t)\right\rangle = \left\langle o_1(t)\widehat{o}_1^{(\mathrm{in})}(t)\right\rangle = 0, \quad (13)$$

$$\left\langle \widehat{o}_2^{(\mathrm{in})}(t)\widehat{o}_2^{(\mathrm{in})}(t)\right\rangle = \left\langle \left(\widehat{o}_1^{(\mathrm{in})}\right)^{*}(t)\widehat{o}_2^{(\mathrm{in})}(t)\right\rangle = 0, \quad (14)$$

$$\left\langle o_1^{*}(t)\widehat{o}_1^{(\mathrm{in})}(t)\right\rangle + \left\langle o_1\left(\widehat{o}_1^{(\mathrm{in})}\right)^{*}(t)\right\rangle = 2\Sigma_1+\kappa\bar{N}_{th}, \quad (15)$$

$$\left\langle o_2^{*}(t)\widehat{o}_2^{(\mathrm{in})}(t)\right\rangle + \left\langle o_2(t)\left(\widehat{o}_2^{(\mathrm{in})}\right)^{*}(t)\right\rangle = \kappa\bar{N}_{th}, \quad (16)$$

$$\left\langle o_2(t)\widehat{o}_1^{(\mathrm{in})}(t)\right\rangle + \left\langle o_1(t)\widehat{o}_2^{(\mathrm{in})}(t)\right\rangle = -2\Sigma_4. \quad (17)$$

We note that Equations (13)-(17) represent the correlation properties of the noise forces $\widehat{o}_1^{(\mathrm{in})}(t)$ and $\widehat{o}_2^{(\mathrm{in})}(t)$ associated with the normal ordering.

It is known that the expectation values of Equations (11) and (12) are identical to Equations (A.2) and (A.3). It is now convenient to introduce a parameter η which relates the probabilities of atoms populating in the bottom and top levels as

$$\rho_l(0) = \frac{(1-\eta)}{2}, \quad (18)$$

provided that $-1 \le \eta \le 1$. Hence, using the fact that $\rho_l(0) + \rho_n(0) = 1$ and Equation (19), it is not subtle to verify that

$$\rho_n(0) = 1-\rho_l(0) = \frac{1+\eta}{2}, \quad (19)$$

$$\rho_{\ln}(0) = \sqrt{\rho_l(0)\rho_n(0)} = \frac{1}{2}\sqrt{1-\eta^2}. \quad (20)$$

Hence, employing Equations (13)-(17) along with (18)-(20) into Equations (11) and (12), we obtain

$$\frac{d}{dt}o_1 = -\xi_{+}o_1-\eta_{+}o_2^{*}+\widehat{o}_1^{(\mathrm{in})}, \quad (21)$$

$$\frac{d}{dt}o_2^{*} = -\xi_{-}o_2^{*}-\eta_{-}o_1+\left(\widehat{o}_2^{(\mathrm{in})}\right)^{*}, \quad (22)$$

where

$$\begin{aligned}\xi_{+} &= \frac{1}{2}(\kappa-2\Sigma_1),\\ \xi_{-} &= \frac{1}{2}(\kappa+2\Sigma_2),\\ \eta_{+} &= -\frac{1}{2}\Sigma_3,\\ \eta_{-} &= \frac{1}{2}\Sigma_4.\end{aligned} \quad (23)$$

We find the solutions of the coupled differential Equations (21)-(22) as the following:

$$\begin{aligned} o_1(t+\tau) &= M_+(\tau)o_1(t) + N_+(\tau)o_2^*(t) + H_+, \\ o_2(t+\tau) &= M_-(\tau)o_2(t) + N_-(\tau)o_1^*(t) + H_-, \end{aligned} \tag{24}$$

in which $H_\pm = I_\pm(t+\tau) + J_\pm(t+\tau)$,
where

$$M_\pm(\tau) = \frac{1}{2}\left[(1 \pm w)e^{-\lambda_-\tau} + (1 \mp w)e^{-\lambda_+\tau}\right], \tag{25}$$

$$N_\pm(\tau) = \frac{y_\pm}{2}\left[e^{-\lambda_+\tau} - e^{-\lambda_-\tau}\right], \tag{26}$$

$$I_+(t+\tau) = \int_0^\tau \left[M_+\left(\tau - \tau'\right)\right]\widehat{o}_1^{(\mathrm{in})}\left(t+\tau'\right)d\tau', \tag{27}$$

$$I_-(t+\tau) = \int_0^\tau \left[M_-\left(\tau - \tau'\right)\right]\widehat{o}_2^{(\mathrm{in})}\left(t+\tau'\right)d\tau', \tag{28}$$

$$J_+(t+\tau) = \int_0^\tau \left[N_+\left(\tau - \tau'\right)\right]\left(\widehat{o}_2^{(\mathrm{in})}\right)^*\left(t+\tau'\right)d\tau', \tag{29}$$

$$J_-(t+\tau) = \int_0^\tau \left[N_-\left(\tau - \tau'\right)\right]\left(\widehat{o}_1^{(\mathrm{in})}\right)^*\left(t+\tau'\right)d\tau', \tag{30}$$

in which

$$\begin{aligned} w &= \frac{\chi_1}{V}, \\ y_\pm &= \frac{-\left[\chi_1\left(\sqrt{\chi_1 - 1}/2\right)\right] \mp \left[\left(3\eta\sqrt{\chi_1 - 1}/2\right) - \chi_2\right]}{V}, \\ V &= \sqrt{(\chi_1)^2 + \left(\frac{\sqrt{\chi_1 - 1}}{2}(\chi_1) - \left(\frac{3\eta\sqrt{\chi_1 - 1}}{2}\right) - \chi_2\right)}, \\ \lambda_+ &= \frac{1}{2}\left[(\xi_+ + \xi_-) + \sqrt{(\xi_+ - \xi_-)^2 + 4\eta_+\eta_-}\right], \\ \lambda_- &= \frac{1}{2}\left[(\xi_+ + \xi_-) - \sqrt{(\xi_+ - \xi_-)^2 + 4\eta_+\eta_-}\right], \end{aligned} \tag{31}$$

where

$$\begin{aligned} \chi_1 &= 1 + \varepsilon^2, \\ \chi_2 &= \sqrt{1 - \eta^2}\left(1 - \frac{\varepsilon^2}{2}\right), \\ \xi_+ &= \frac{1}{2}(\kappa - 2\Sigma_1), \\ \xi_- &= \frac{1}{2}(\kappa + 2\Sigma_2), \\ \eta_+ &= -\frac{1}{2}\Sigma_3, \\ \eta_- &= \frac{1}{2}\Sigma_4. \end{aligned} \tag{32}$$

3. Quantum Steering via Coherent Classical Field

Quantum steering refers to the nonclassical correlations that can be observed between the outcomes of measurements applied on half of an entangled state and the resulting post-measured states that are left with the other party. From an operational point of view, a steering test can be seen as an entanglement test where one of the parties performs uncharacterised measurements. Thus, quantum steering is a form of quantum inseparability that lies in between the well-known notions of the Bell nonlocality and entanglement. It is a quantum correlation that can exist if and only if the system is entangled. Therefore, it is stronger than entanglement. Let us consider local Gaussian measurements performed on mode $\widehat{o}_1$. A Gaussian state, $\widehat{\rho} = \rho(\widehat{o}_1, \widehat{o}_2)$ for two-mode photons, is $\widehat{o}_1 \longrightarrow \widehat{o}_2$ steerable if the following condition is violated [18, 22, 23]:

$$L + i\left(0_{\widehat{o}_1} \oplus \Omega_{\widehat{o}_2}\right) \geq 0, \tag{33}$$

in which $\Omega_{\widehat{o}_2}$ is the covariance matrix pure states in the second system described by

$$\begin{aligned} \Omega_{\widehat{o}_2} &= \oplus_1^2 \begin{pmatrix} 0 & 1 \\ -1 & 0 \end{pmatrix}, \\ L &= \begin{pmatrix} L_1 & L_{12} \\ L_{12}^T & L_2 \end{pmatrix} \end{aligned} \tag{34}$$

is the covariance matrix of photon pairs, and $0_{\widehat{o}_1}$ indicates the null matrix in the first system.

It is a common knowledge that Equation (33) is satisfied when $L_1 > 0$ and $(L_2 - L_{12}^T L_1^{-1} L_{12}) + i\Omega_{o_2} \geq 0$. The first condition $L_1 > 0$ is always true since the operator representing these measurements is a positive covariance matrix. Therefore, L is $\widehat{o}_1 \longrightarrow \widehat{o}_2$ steerable only if the second condition is violated. That is, when the matrix

$$L_L^2 + i\Omega_{o_2} < 0, \tag{35}$$

where $L_L^2 = (L_2 - L_{12}^T L_1^{-1} L_{12})$.

The symmetric matrix L_L^2 can be diagonalized using symplectic transformations that yield physically interesting symplectic eigenvalues of L_L^2, which we have already derived as $(s_\pm)^2 = (a \pm \sqrt{a^2 - 4\det(L)})/2$, where $a = \det(L_1) + \det(L_2) + 2\det(L_{12})$ and $s_\pm$ are invariant quantities. In terms of these eigenvalues, $\widehat{o}_1 \longrightarrow \widehat{o}_2$ steerability is given by

$$S^{\widehat{o}_1 \longrightarrow \widehat{o}_2} = \left[0, \frac{1}{2}\ln\left(\frac{\det[L_1]}{4\det[L]}\right)\right]. \tag{36}$$

Quantum steering is asymmetric since it is one-way and device-independent quantum correlation. Therefore, one could easily swap the roles of L_1 and L_2 to obtain the measurement of Gaussian quantum steering, $S^{\widehat{o}_2 \longrightarrow \widehat{o}_1}$. According

to these formulations, Gaussian quantum steering is exhibited only when $S^{\hat{o}_1 \longrightarrow \hat{o}_2} > 0$ and $S^{\hat{o}_2 \longrightarrow \hat{o}_1} > 0$. However, there would be no information on the upper bounds. This may be an issue to correctly measure the degree of quantum steering.

Therefore, we follow another formalism in which case, the necessary and sufficient condition for two-mode Gaussian quantum steer-ability from $\hat{o}_1 \longrightarrow \hat{o}_2$ is

$$S^{\hat{o}_1 \longrightarrow \hat{o}_2} = \Delta x_{3|1} \Delta x_{4|2} < 1. \tag{37}$$

Here, the conditional variances are defined by $[\Delta x_{3|1}]^2 = [\Delta(x_3 - g_x x_1)]^2$ and $[\Delta x_{4|2}]^2 = [\Delta(x_4 + g_p x_2)]^2$, in which g_x and g_p are optimization factors which are real constants adjustable to minimize quantum fluctuations corresponding to the previously defined quadrature operators. After detailed mathematical manipulation in the optimization conditions, we arrived at

$$\left(S^{\hat{o}_1 \longrightarrow \hat{o}_2}\right)^2 = \left[l_{11}(t) - \frac{l_{13}^2(t)}{l_{33}(t)}\right]\left[l_{11}(t) - \frac{l_{24}^2(t)}{l_{33}(t)}\right], \tag{38}$$

with the optimization factors $g_x = l_{13}(t)/l_{33}(t)$ and $g_p = -l_{24}(t)/l_{33}(t)$.

To investigate $S^{\hat{o}_1 \longrightarrow \hat{o}_2}$ and $S^{\hat{o}_2 \longrightarrow \hat{o}_1}$, we plot $S^{\hat{o}_1 \longrightarrow \hat{o}_2}$ and $S^{\hat{o}_2 \longrightarrow \hat{o}_1}$ versus the dimensionless parameter ξ/γ by varying the relevant system parameters. An in-depth analysis of quantum steering and its comparison with other quantum features can be made using 2D plots as follows. Figures 2 and 3 depict the variation of the quantum steering with coherent classical fields and the parameters characterizing the system as a whole. We also notice that the quantum steering declines with increased temperature of the heat bath describing via $\bar{n}_{th}$ and phase fluctuations. On the other hand, injecting more atoms quickly into the cavity and tuning the coherent classical field to an appropriate intensity can efficiently oppose the negative impact of quantum decoherences to generate one-way quantum steering from $S^{\hat{o}_1 \longrightarrow \hat{o}_2}$. It is a peculiar behavior of the manifested quantum steering that disappears in the strong coupling regime, where notable quantum discord and entanglement are observed under the same system parameters. This must be attributed to the quantum coherence built up by a coherent classical field in the strong coupling regime which is not strong enough to generate quantum steering, which is one of the restrictive nature of quantum correlations.

4. Quantum Steering via Coherent Superposition

Dependence of one-way Gaussian quantum steering on $S^{\hat{o}_1 \longrightarrow \hat{o}_2}$ is demonstrated in Figures 4–6 under different system parameters. From these figures, $S^{\hat{o}_1 \longrightarrow \hat{o}_2} \geq 1$ for $\eta = 1$, in which the superposition-induced atomic coherence vanishes completely since all atoms occupy at the ground energy level with 100% probability. The maximum achievable strength of quantum steering occurs when atoms are found with 48.5% of the excited energy level, for which other quantum features are also stronger. We also observe a rapid increase of the strength of quantum steering with increased atomic injection rates. However, after attaining its peak value, quantum steering rapidly decreases with an increased probability of the atoms in the ground energy level. One can also see that the quantum steering decreases with the temperature of the heat bath and atomic phase fluctuations.

5. Quantum Entanglement via Coherent Classical Field

A pair of quantum mechanical particles is in an entangled state if and only if their individual states cannot be expressed as a product of the states of its separate constituents. Thus, one can write

$$\hat{\rho} \neq \sum_i P_i \hat{\rho}_i^{(1)} \otimes \hat{\rho}_i^{(2)}, \tag{39}$$

where $P_i \geq 0$ and $\sum_i P_i = 1$ represent the normalization condition for the combined density state of the composite system.

Although numerous criteria of entanglement measures have been developed and currently available in the literature, here, we apply the criterion set by Duan et al. [24]. This criterion is highly interesting due to its direct utilization to quantify quantum squeezing.

Based on this criterion, a quantum state of the system is entangled if the sum of the variances of the EPR-type operators $\hat{x}$ and $\hat{p}$ satisfies the condition:

$$\frac{\Delta x^2 + \Delta p^2}{2} < 1, \tag{40}$$

in which $\hat{x} = \hat{x}_a - \hat{x}_b$ and $\hat{p} = \hat{p}_a + \hat{p}_b$. Here, $\hat{x}_a = (1/\sqrt{2})(\hat{o}_1^\dagger + \hat{o}_1)$, $\hat{x}_b = (1/\sqrt{2})(\hat{o}_2^\dagger + \hat{o}_2)$, $\hat{p}_a = (i/\sqrt{2})(\hat{o}_1^\dagger - \hat{o}_1)$, and $\hat{p}_b = (i/\sqrt{2})(\hat{o}_2^\dagger - \hat{o}_2)$ are the quadrature operators of the cavity-mode photons.

Now, we find the variances of $\hat{x}$ and $\hat{p}$. The variance $\hat{x}$ can be obtained from the relation $\Delta x^2 = \langle x^2 \rangle - \langle x \rangle^2$, where

$$\begin{aligned}\langle x^2 \rangle = \frac{1}{2}\big[2 + 2\langle \hat{o}_1^\dagger \hat{o}_1 \rangle + 2\langle \hat{o}_2^\dagger \hat{o}_2 \rangle - \big(\langle \hat{o}_1 \hat{o}_2 \rangle \\ + \langle \hat{o}_1^\dagger \hat{o}_2^\dagger \rangle + \langle \hat{o}_2 \hat{o}_1 \rangle + \langle \hat{o}_2^\dagger \hat{o}_1^\dagger \rangle\big)\big].\end{aligned} \tag{41}$$

It is now not difficult to find Equation (41); it reads as follows:

$$\langle x^2 \rangle = \frac{1}{2}[2 + 2\langle o_1^* o_1 \rangle + 2\langle o_2^* o_2 \rangle - 4\langle o_1 o_2 \rangle]. \tag{42}$$

Moreover, it is straightforward to see that

$$\langle x \rangle^2 = 0. \tag{43}$$

With the help of Equations (41) and (43), the variance of $\hat{x}$ becomes:

$$\Delta x^2 = \langle x^2 \rangle = 1 + \langle o_1^* o_1 \rangle + \langle o_2^* o_2 \rangle - 2\langle o_1 o_2 \rangle. \tag{44}$$

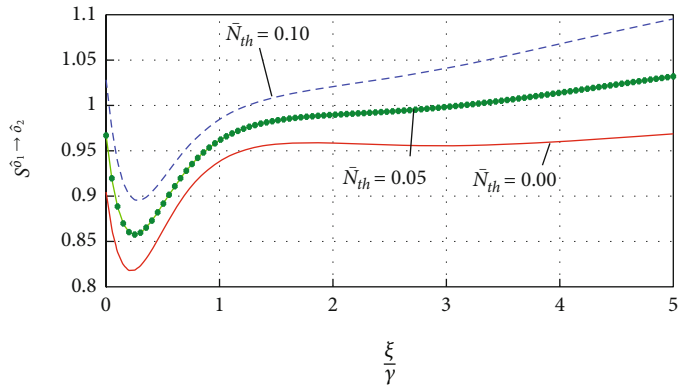

FIGURE 2: Time evolution of quantum steering $S^{\hat{o}_1 \to \hat{o}_2}$ against coherent-induced classical field for $r_a = 2$ kHz, $\kappa = 0.5$ kHz, $\eta = 0.1$, $g = 0.8\gamma$, $t = 10$ s, $\theta = 0.001$, and $\bar{N}_{th} = 0.00$, 0.05, and 0.1.

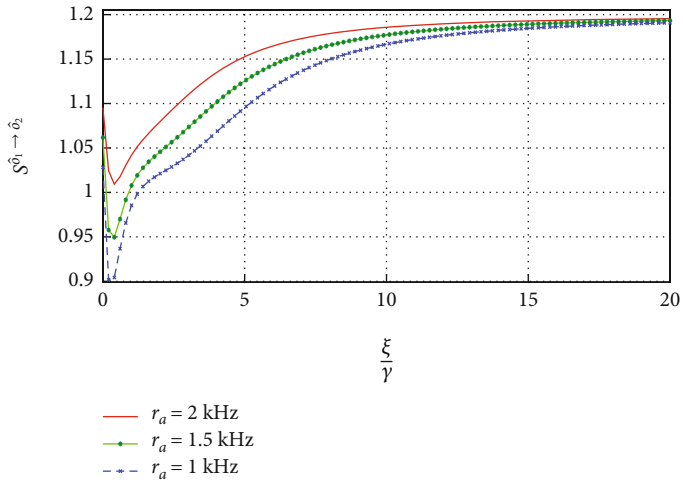

FIGURE 3: Time evolution of quantum steering $S^{\hat{o}_1 \to \hat{o}_2}$ against coherent-induced classical field for $\bar{N}_{th} = 0.1$, $\kappa = 0.5$ kHz, $\eta = 0.1$, $g = 0.8\gamma$, $t = 10$ s, $\theta = 0.001$, and $r_a = 1$ kHz, 1.5 kHz, and 2 kHz.

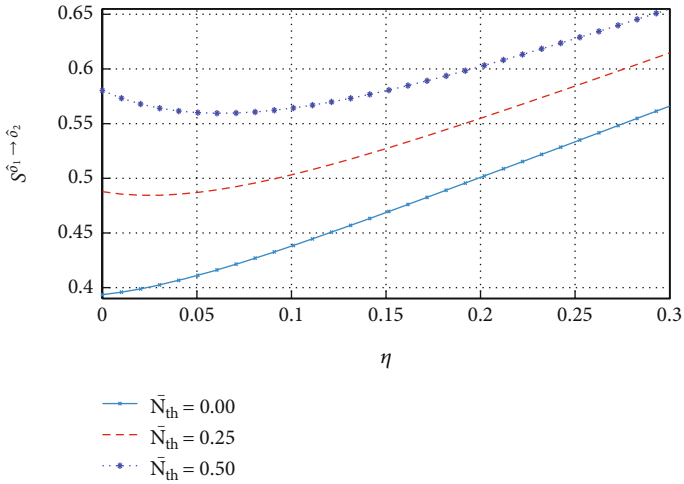

FIGURE 4: Time evolution of quantum steering $S^{\hat{o}_1 \to \hat{o}_2}$ against atomic state superposition $r_a = 10$ kHz, $\kappa = 0.5$ kHz, $t = 10$ s, $g = 0.8\gamma$, $\xi = 0.1\gamma$, $\theta = 0.001$, and $\bar{N}_{th} = 0.00$, 0.25, and 0.5.

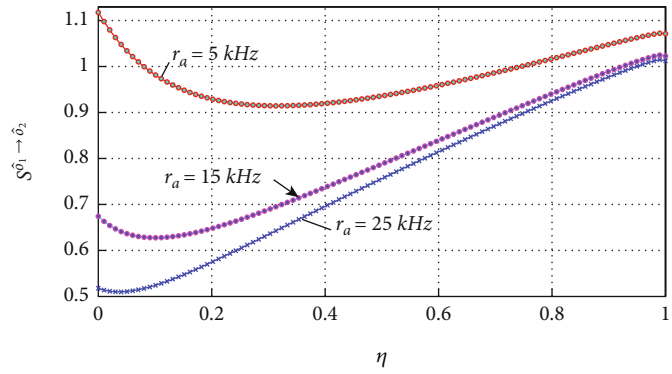

FIGURE 5: Time evolution of quantum steering $S^{\hat{o}_1 \longrightarrow \hat{o}_2}$ against atomic state superposition $\bar{N}_{th} = 0.5$, $\kappa = 0.5$ kHz, $t = 10$ s, $g = 0.8\gamma$, $\xi = 0.1\gamma$, $\theta = 0.001$, and $r_a = 5$ kHz, 15 kHz, and 25 kHz.

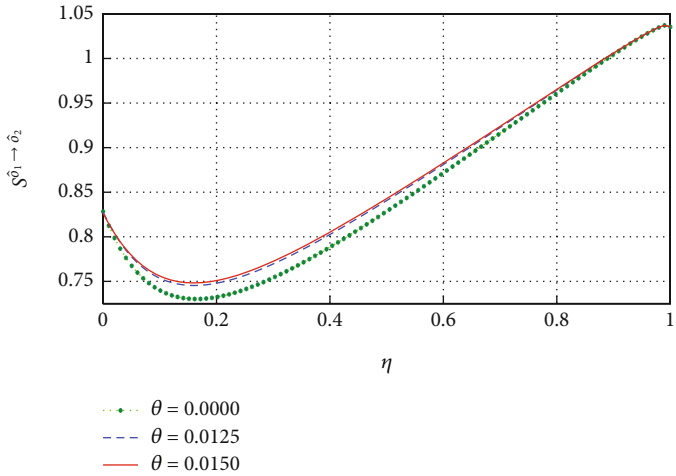

FIGURE 6: Time evolution of quantum steering $S^{\hat{o}_1 \longrightarrow \hat{o}_2}$ against atomic state superposition for $\bar{N}_{th} = 0.5$, $\kappa = 0.5$ kHz, $t = 10$ s, $g = 0.8\gamma$, $\xi = 0.1\gamma$, $r_a = 10$ kHz, and $\theta = 0.00$, 0.0125, and 0.015.

Following the same procedure, it is possible to verify that

$$\Delta p^2 = 1 + \langle o_1^* o_1 \rangle + \langle o_2^* o_2 \rangle - 2\langle o_1 o_2 \rangle. \tag{45}$$

Thus, the sum of the variances of $\hat{x}$ and $\hat{p}$ is found to be

$$\frac{\Delta x^2 + \Delta p^2}{2} = 1 + \bar{n}_1(t) + \bar{n}_2(t) - 2\bar{n}_{12}(t), \tag{46}$$

where $\bar{n}_1 = \langle o_1^* o_1 \rangle$, $\bar{n}_2 = \langle o_2^* o_2 \rangle$, and $\bar{n}_{12} = \langle o_1 o_2 \rangle$ are clearly given by Equations (A.17)-(A.20). To investigate the entanglement of the two-mode radiation with this criterion, $(\Delta x^2 + \Delta p^2)/2$ is plotted for the same system parameters used in the previous section. The quantum system exhibits 100% entangled and nonentangled when the sum of fluctuations in the position and momentum-like operators reduces to zero, $(\Delta x^2 + \Delta p^2)/2 = 0$, and greater than one, $(\Delta x^2 + \Delta p^2)/2 > 1$, respectively.

The dependence of quantum entanglement on time, coherent classical field, and coherent superposition can be inferred from Figures 6 and 7. Variation of quantum entanglement with coherent classical fields under different system parameters is demonstrated in Figures 7–9, in which the quantum entanglement is lost between $\xi = 3\gamma/4$, and $\xi = 6\gamma$. However, it increases for certain values of the parameter of the coherent-induced classical field and attains peak values around $\xi = \gamma/10$ and $\xi = 10\gamma$. We show that the photon pairs are in a maximally entangled state boosted with an increased atomic injection rate. For the same system parameters, the quantum discord states for light modes are also strong. This would probably be one of the interesting results of our system for it can simultaneously support entangled state or discordant state-based quantum information processing. On the other side, the photon pairs are in a slightly changing entangled state, which could vary depending on other units of quantum system, for $\xi > 10\gamma$. However, the entanglement declines with increasing parameters of quantum decoherences heat bath and atomic phase fluctuation.

6. Quantum Entanglement via Coherent Superposition

The effect of atomic state superposition on the dynamics of quantum entanglement is shown in Figures 10–12. The influences of system parameters such as time, phase fluctuations,

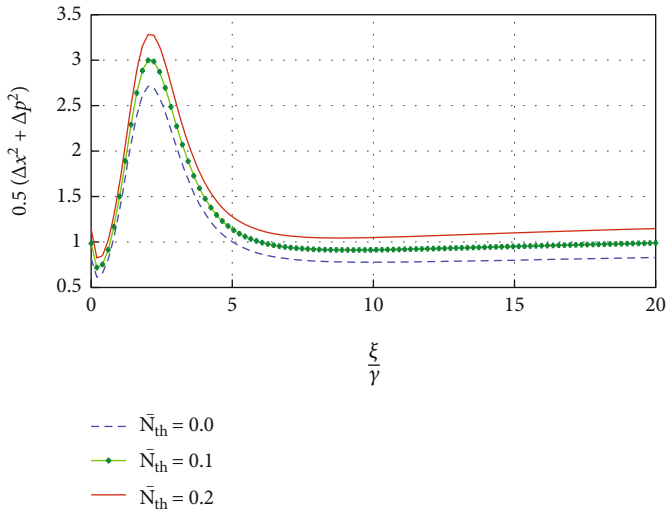

Figure 7: Quantum entanglement $(\Delta x^2 + \Delta p^2)/2$ of the photon pairs against coherent-induced classical field for $r_a = 2$ kHz, $\kappa = 0.5$ kHz, $\eta = 0.1$, $g = 0.8\gamma$, $t = 10$ s, $\theta = 0.001$, and $\bar{N}_{th} = 0.00$, 0.1, and 0.2.

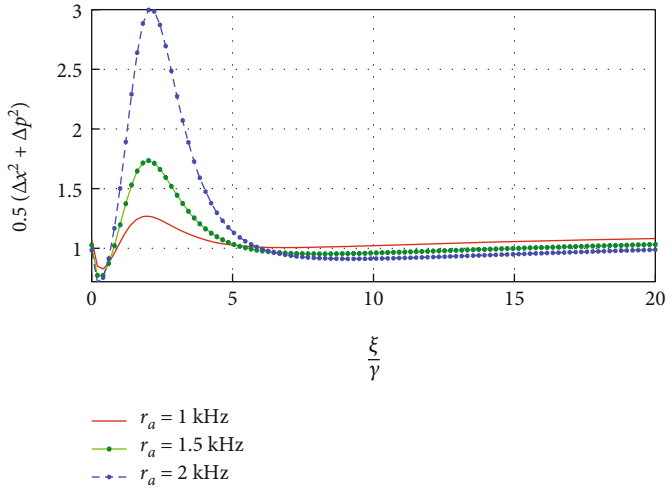

Figure 8: Quantum entanglement $(\Delta x^2 + \Delta p^2)/2$ of the photon pairs against coherent-induced classical field for $\bar{N}_{th} = 0.1$, $\kappa = 0.5$ kHz, $\eta = 0.1$, $g = 0.8\gamma$, $t = 10$ s, $\theta = 0.001$, and $r_a = 1$ kHz, 1.5 kHz, and 2 kHz.

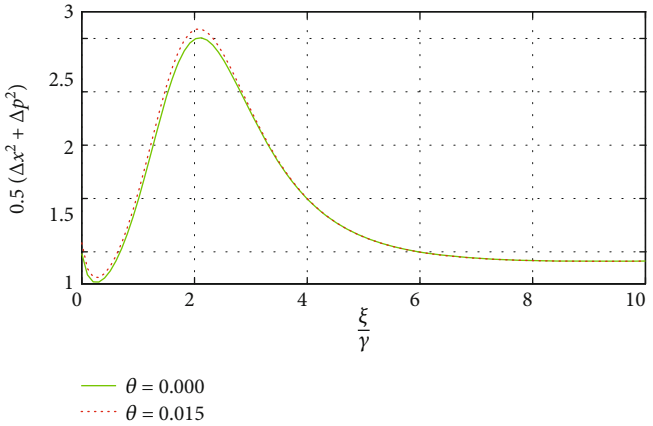

Figure 9: Quantum entanglement $(\Delta x^2 + \Delta p^2)/2$ of the photon pairs against coherent-induced classical field for $\bar{N}_{th} = 0.1$, $\kappa = 0.5$ kHz, $\eta = 0.1$, $g = 0.8\gamma$, $t = 10$ s, $r_a = 2$ kHz, and $\theta = 0.00$ and 0.015.

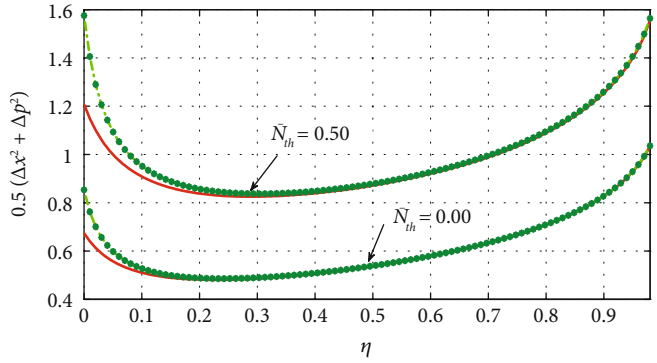

FIGURE 10: Quantum entanglement $(\Delta x^2 + \Delta p^2)/2$ of the photon pairs against atomic state superposition for $r_a = 10$ kHz, $\kappa = 0.5$ kHz, $t = 10$ s, $g = 0.8\gamma$, $\xi = 0.1\gamma$, $\theta = 0.001$, and $\bar{N}_{th} = 0.00$ and 0.5: at steady state (dashed curve) and $t = 10$ s (solid curve) and at $t = 10$ s.

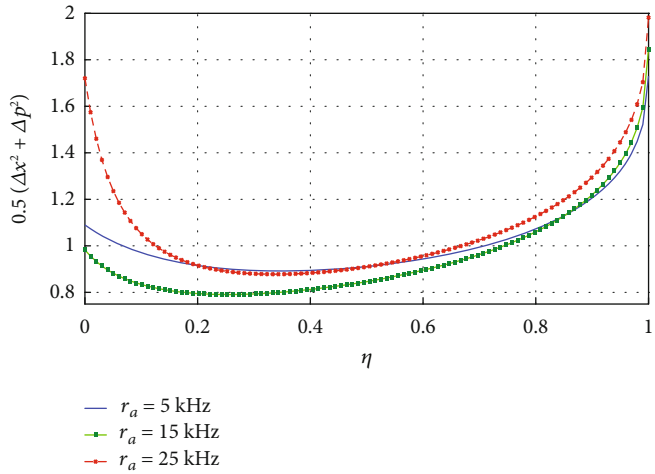

FIGURE 11: Quantum entanglement $(\Delta x^2 + \Delta p^2)/2$ of the photon pairs against atomic state superposition for $\bar{N}_{th} = 0.5$, $\kappa = 0.5$ kHz, $t = 10$ s, $g = 0.8\gamma$, $\xi = 0.1\gamma$, $\theta = 0.001$, and $r_a = 5$ kHz, 15 kHz, and 25 kHz.

and atomic injection rate on the dynamics of entanglement are negligible for $\eta = 1$ but considerable for $\eta = 0$. Entanglement of photon pairs is maximized near the maximum atomic coherence, $\eta = 0.23$, and enhanced with the help of r_a as shown in Figure 11. Under the same condition, the entanglement of photon pairs at $t = 10$ s is more by 20% than that at a steady state for $\eta = 0$ and $\bar{N}_{th} = 0$ (see Figure 10). On the other hand, we show in Figure 12 that the entanglement of photon pairs is completely lost by small phase fluctuations of $\theta \geq 0.0125$. Therefore, the investigation of quantum features without considering phase fluctuations is just an assumption far from participial reality.

7. Quantum Discord via Coherent Classical Field

Quantum discord is defined as a measure of the quantum correlations present in a system. The difference arises because of the role played by measurement on the system. Quantum discord has been of relevant research interest during the past few decades in light of its potential as a resource of quantum information and communication, especially in disentangled quantum systems.

In the classical systems, it is possible to obtain all information of the system without disturbing it. However, this is not the case in quantum mechanics since measurements can in general modify quantum systems. Owing to this fact, the two equivalent expressions of mutual information in classical information theory are not the same for quantum systems. The difference between these equivalent quantities is used to define the quantum discord $D^{\hat{o}_1}$, which is a quantum correlation beyond entanglement, given by

$$D^{\hat{o}_1} = I(\hat{\rho}) - \max_{\prod_B} [J(\hat{\rho})], \tag{47}$$

where $\hat{\rho} = \rho(\hat{o}_1, \hat{o}_2)$ represents the density operator of the combined system, and

$$I(\hat{\rho}) = S(\hat{o}_1) + S(\hat{o}_2) - S(\hat{\rho}) \tag{48}$$

is the quantum mutual information that provides a measure of the total correlation within a bipartite system. In this descriptions, $S(\hat{o}_1)$ and $S(\hat{o}_2)$ represent the Von Neumann entropy of each mode while $S(\hat{\rho})$ is the joint Von Neumann

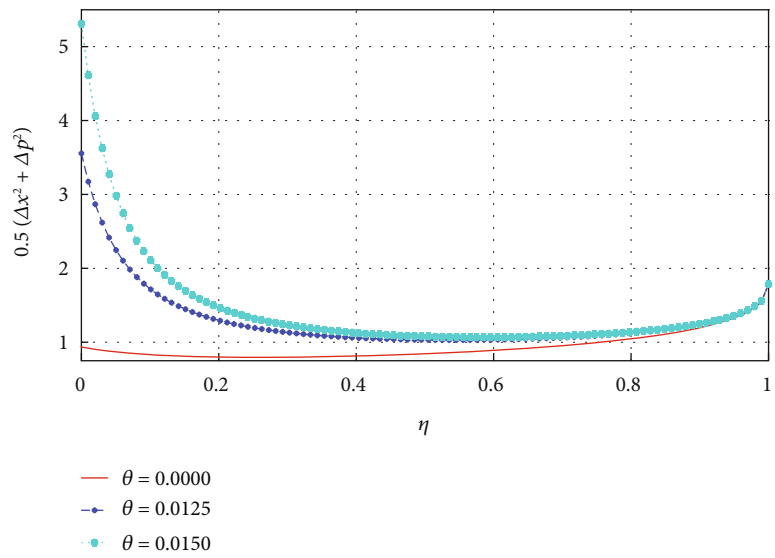

FIGURE 12: Quantum entanglement $(\Delta x^2 + \Delta p^2)/2$ of the photon pairs against atomic state superposition for $\bar{N}_{th} = 0.5$, $\kappa = 0.5$ kHz, $t = 10$ s, $g = 0.8\gamma$, $\xi = 0.1\gamma$, $r_a = 10$ kHz, and $\theta = 0.00$, 0.0125, and 0.015.

entropy of the bipartite system. On the other hand, $J(\widehat{\rho})$ represents the classical mutual information that captures the classical correlations given by [25] $J(\widehat{\rho}) = S(\widehat{o}_1) - S(\widehat{\rho}(\widehat{o}_1, \widehat{o}_2)|\prod_{\widehat{o}_2}^{j})$. Here, the term $S(\widehat{\rho}(\widehat{o}_1, \widehat{o}_2)|\prod_{\widehat{o}_2}^{j})$ indicates that the conditional Von Neumann entropy of modes $\widehat{o}_1$ and $\widehat{o}_2$, with $\prod_{\widehat{o}_2}^{j} = |j_{\widehat{o}_2}\rangle\langle j_{\widehat{o}_2}|$ being a set of local projective measurements on light mode $\widehat{o}_2$. An optimization condition should be imposed on $J(\widehat{\rho})$ to avoid the dependence of quantum discord on the measurements [26, 27]. This reads as follows:

$$\max_{\prod_B^j} [J(\widehat{\rho})] = S(\widehat{o}_1) - \min_{\prod_B^j} \left[S\left(\widehat{\rho}(\widehat{o}_1, \widehat{o}_2) \middle| \prod_{\widehat{o}_2}^{j} \right) \right]. \quad (49)$$

The optimization process of measurement of mutual information highly complicates the quantification of quantum discord in general. Analytical formulas of quantum discord are derived for continuous variable Gaussian bipartite systems in Refs. [28, 29]. Continuous variable Gaussian states have Gaussian Wigner functions. It is well known that a bipartite Gaussian system is fully described by its symplectic eigenvalues, covariance matrix, and the standard form of diagonal subblocks. This reads as follows:

$$L = \begin{pmatrix} L_1 & L_{12} \\ L_{12}^T & L_2 \end{pmatrix}, \quad (50)$$

in which L_1 and L_2 are the covariance matrices describing each mode separately, while L_{12} are the intermodal correlations. The elements of the matrix in Equation (27) can be obtained from the relation [29]

$$L_{ij} = \frac{1}{2}\langle \widehat{x}_i \widehat{x}_j + \widehat{x}_j \widehat{x}_i \rangle - \langle \widehat{x}_i \rangle \langle \widehat{x}_j \rangle, \quad (51)$$

in which $i, j = 1, 2, 3, 4$. The quadrature operators are defined as $\widehat{x}_1 = \widehat{o}_1 + \widehat{o}_1^{\dagger}$, $\widehat{x}_2 = i(\widehat{o}_1^{\dagger} - \widehat{o}_1)$, $\widehat{x}_3 = \widehat{o}_2 + \widehat{o}_2^{\dagger}$, and $\widehat{x}_4 = i(\widehat{o}_2^{\dagger} - \widehat{o}_2)$. Using these definitions, the only nonvanishing terms in the extended covariance matrix are

$$L = \begin{pmatrix} l_{11}(t) & 0 & l_{13}(t) & 0 \\ 0 & l_{22}(t) & 0 & l_{24}(t) \\ l_{31}^*(t) & 0 & l_{33}(t) & 0 \\ 0 & l_{42}^*(t) & 0 & l_{44}(t) \end{pmatrix}, \quad (52)$$

where $l_{11}(t) = l_{22}(t) = \sqrt{\det(L_1)} = 2n_1(t) + 1$, $l_{33}(t) = l_{44}(t) = \sqrt{\det(L_2)} = 2n_2(t) + 1$, and $l_{13}(t) = -l_{24}(t) = \sqrt{-\det(L_{12})} = 2n_{12}(t)$. One can also easily verify that

$$\det(L) = [l_{11}(t) l_{33}(t) + l_{13}(t) l_{24}(t)]^2. \quad (53)$$

On the other hand, the corresponding eigenvalues of the symplectic matrix described in Equation (51) are given by

$$(s_{\pm})^2 = \frac{a \pm \sqrt{a^2 - 4\det(L)}}{2}, \quad (54)$$

where $a = \det(L_1) + \det(L_2) + 2\det(L_{12})$ and $s_{\pm}$ are invariant quantities.

The continuous variable Gaussian quantum discord for two-mode radiation described by a covariance matrix M is given by

$$D^{\widehat{o}_1} = I(l_{33}(t)) - I(s_-) - I(s_+) + I\left(\sqrt{\Gamma}\right), \quad (55)$$

where

$$\Gamma = \begin{cases} \dfrac{2(l_{13})^4 + \left[(l_{33})^2 - 1\right]\left[\det(L) - (l_{11})^2\right] + 2\left|l_{13}^2\right|\sqrt{(l_{13})^4 + \left[(l_{33})^2 - 1\right]\left[\det(L) - (l_{11})^2\right]}}{\left[(l_{33})^2 - 1\right]^2} & \text{if } c \geq 0, \\ \dfrac{(l_{11}l_{33})^2 - (l_{13})^4 + \det(L) - \sqrt{(l_{13})^8 + \left[\det(L) - (l_{11}l_{33})^2\right]^2 - 2(l_{13})^4\left[\det(L) + (l_{11}l_{33})^2\right]}}{2(l_{33})^2} & \text{if } c < 0, \end{cases} \tag{56}$$

with $c = [(l_{11})^2 + 1][\det(L) + (l_{33})^2] - [\det(L) - (l_{11}l_{33})^2]^2$, and we also note that for any variable x, the function $I(x)$ is defined by $I(x) = ((1+x)/2)\log_2((1+x)/2) - ((1-x)/2)\log_2((1-x)/2)$. In these equations, we have not shown time dependence to save environment.

The quantum discord for mode $\hat{o}_2$ can be easily obtained by swapping the role of $l_{11}(t)$ and $l_{33}(t)$. This reads as follows:

$$D^{\hat{o}_2} = I(l_{11}(t)) - I(s_-) - I(s_+) + I\left(\sqrt{\Gamma'}\right), \tag{57}$$

where

$$\Gamma' = \begin{cases} \dfrac{2(l_{13})^4 + \left[(l_{11})^2 - 1\right]\left[\det(L) - (l_{33})^2\right] + 2\left|l_{13}^2\right|\sqrt{(l_{13})^4 + \left[(l_{11})^2 - 1\right]\left[\det(L) - (l_{33})^2\right]}}{\left[(l_{11})^2 - 1\right]^2} & \text{if } c \geq 0, \\ \dfrac{(l_{11}l_{33})^2 - (l_{13})^4 + \det(L) - \sqrt{(l_{13})^8 + \left[\det(L) - (l_{11}l_{33})^2\right]^2 - 2(l_{13})^4\left[\det(L) + (l_{11}l_{33})^2\right]}}{2(l_{11})^2} & \text{if } c < 0. \end{cases} \tag{58}$$

According to the definition of quantum discord, two-mode radiation fields are entangled for $D^{\hat{o}_1}(D^{\hat{o}_2}) > 1$, and the two-mode fields can either be in a separable or entangled state for $0 \leq D^{\hat{o}_1}(D^{\hat{o}_2}) < 1$. The effect of coherent classical field interaction on atomic transitions from the excited state and ground state is clearly demonstrated in Figures 13–15. We selected a specific value of system parameters based on the previously realized experimental schemes for microwave setup [24, 30] and recognized the theoretical articles [31]. It is clearly indicated that the quantum discord is stronger in the absence of the coherent classical fields, $\xi = 0$. For $\xi \neq 0$, the classical field begins contributing its part. Quantum discord for mode $\hat{o}_1$ sharply declines with increasing classical field parameters until $\xi \approx \gamma$, then its slowly increases to attain a certain maximum value around at $\xi = 3.5\gamma$, and later, it slowly decreases to zero depending on the values of other parameters such as r_a and $\bar{N}_{th}$. This may occur because the classical field does not induce quantum coherence uniformly, and hence, an appropriate value of its parameter can be chosen to get an optimized quantum discord. This quantum feature can highly be increased by adding temperature of the heat bath and increasing the atomic injection rate (see Figures 13 and 14). Moreover, increasing phase fluctuations could slightly improve the quantum discord as can be seen in Figure 15.

8. Quantum Discord via Coherent Superposition

Dependence of quantum discord for mode $\hat{o}_1$ on the quantum coherence induced by quantum superposition of atomic states has been shown in Figures 16–18 under different system parameters. Analytical calculations have indicated that the quantum coherence induced by the atomic state superposition is maximum for $\eta = 0$ and minimum for $\eta = 1$ (see Equations (19) and (20)). These figures also manifest the same features: quantum discord becomes weak and strong when the quantum coherence induced by atomic state superposition is minimum and maximum, respectively. This must happen due to the fact that quantum coherences are a resource for quantum features including quantum discord.

9. Conclusion

In this paper, we have studied the effect of classical and quantum superposition of atomic states on quantum correlations. The photon pairs were strongly coupled through coherent-induced classical fields and atomic state superposition and were subjected to two different kinds of quantum decoherence due to coupling with heat bath and atomic phase fluctuations. The dynamics of quantum correlations

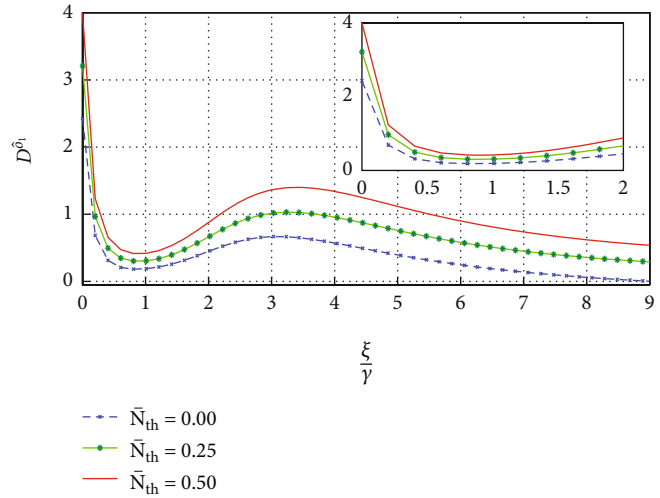

Figure 13: Quantum discord $(D^{\hat{o}_1})$ of light mode $\hat{o}_1$ against coherent-induced classical field for $r_a = 2$ kHz, $\kappa = 0.5$ kHz, $\eta = 0.1$, $g = 0.8\gamma$, $t = 10$ s, $\theta = 0.001$, and $\bar{N}_{th} = 0.00$, 0.25, and 0.5.

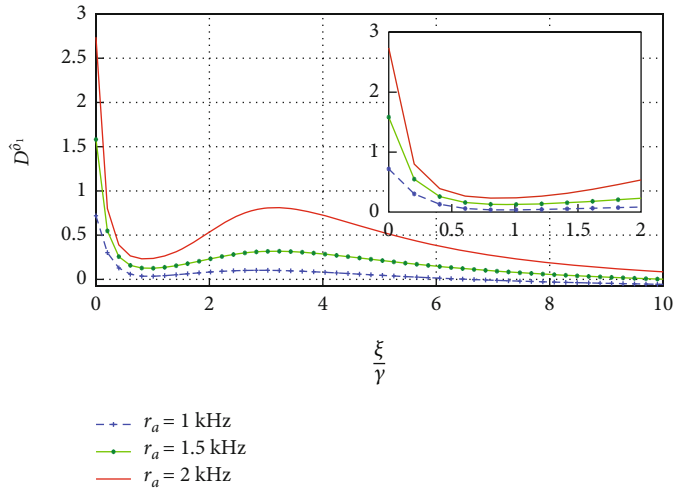

Figure 14: Quantum discord $(D^{\hat{o}_1})$ of light mode $\hat{o}_1$ against coherent-induced classical field for $\bar{N}_{th} = 0.1$, $\kappa = 0.5$ kHz, $\eta = 0.1$, $g = 0.8\gamma$, $t = 10$ s, $\theta = 0.001$, and $r_a = 1$ kHz, 1.5 kHz, and 2 kHz.

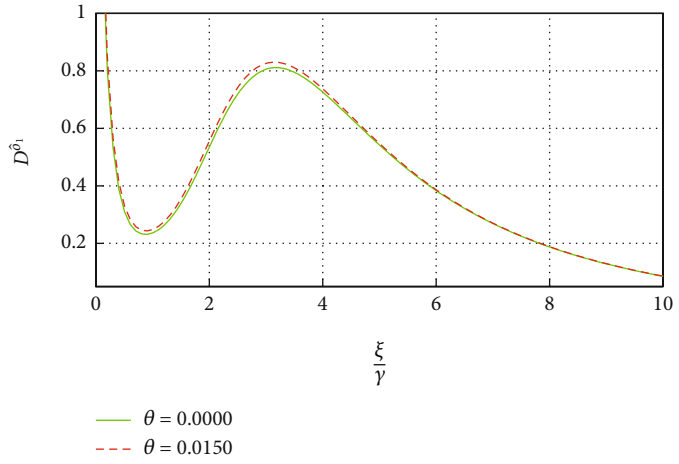

Figure 15: Quantum discord $(D^{\hat{o}_1})$ of light mode $\hat{o}_1$ against coherent-induced classical field for $\bar{N}_{th} = 0.1$, $\kappa = 0.5$ kHz, $\eta = 0.1$, $g = 0.8\gamma$, $t = 10$ s, $r_a = 2$ kHz, and $\theta = 0.00$ and 0.015.

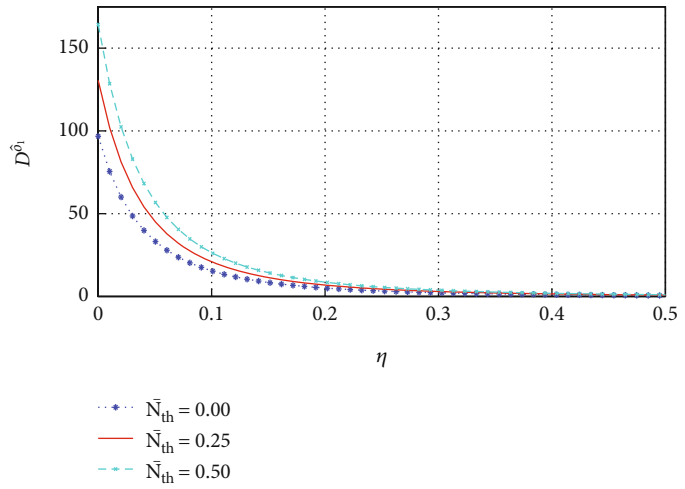

FIGURE 16: Quantum discord $(D^{\hat{o}_1})$ of the light mode $\hat{o}_1$ with the atomic state superposition for $r_a = 10$ kHz, $\kappa = 0.5$ kHz, $t = 10$ s, $g = 0.8\gamma$, $\xi = 0.1\gamma$, $\theta = 0.001$, and $\bar{N}_{th} = 0.00$, 0.25, and 0.5.

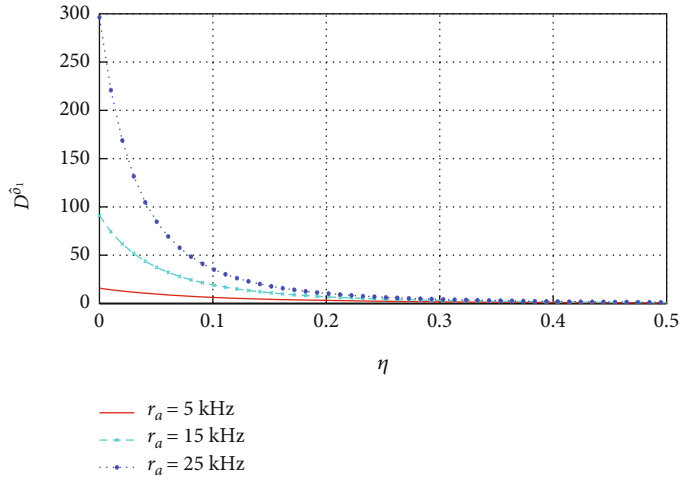

FIGURE 17: Quantum discord $(D^{\hat{o}_1})$ of light mode $\hat{o}_1$ against atomic state superposition for a $\bar{N}_{th} = 0.5$, $\kappa = 0.5$ kHz, $t = 10$ s, $g = 0.8\gamma$, $\xi = 0.1\gamma$, $\theta = 0.001$, and $r_a = 5$ kHz, 15 kHz, and 25 kHz.

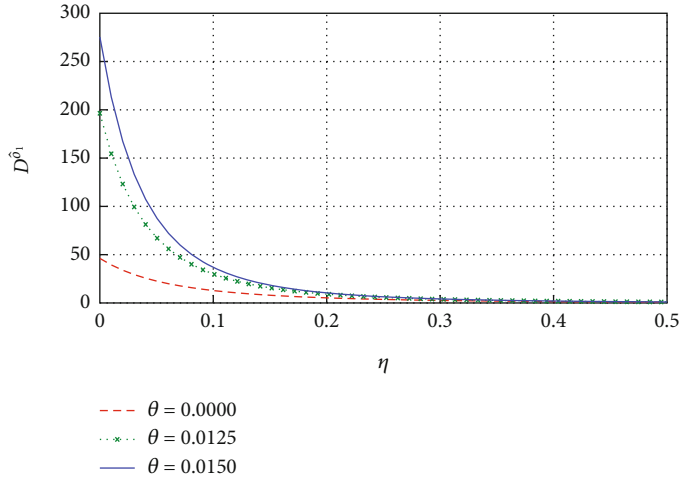

FIGURE 18: Quantum discord $(D^{\hat{o}_1})$ of light mode $\hat{o}_1$ against atomic state superposition for $\bar{N}_{th} = 0.5$, $\kappa = 0.5$ kHz, $t = 10$ s, $g = 0.8\gamma$, $\xi = 0.1\gamma$, $r_a = 10$ kHz, and $\theta = 0.00$, 0.0125, and 0.015.

have been observed and analyzed using the c-number master equations by taking into account different system parameters. The maximum achievable strength of quantum correlation is enhanced by increasing the rate of atomic injection, choosing an appropriate parameter of the coherent-induced classical fields which can adjust the atomic populations to the desired energy levels. The effect of atomic injection rate advances as time goes on and is more effective when 48.5% and 51.5% of atoms populate in the excited and ground energy levels. This result is attributed to the fact that atoms require sufficient time to interact and transfer their coherence to the photon pairs. On the other hand, it has been observed that the classical field is efficiently used up to induce quantum coherence only when sufficient numbers of atoms are available in the excited energy state while pumping the atoms from the ground state to the excited state would be an additional task for it when none of them are initially in the excited state. This is why quantum steering disappears in the strong coupling regime in which notable quantum discord and entanglement are observed under the same system parameters. Perceptible from the quantum discord that increases with quantum decoherence, the quantum entanglement and steering wipe out with increased decoherences originated from the temperature of the heat bath and atomic phase fluctuations. The strength of quantum steering stays for a long period of time under thermal decoherence but slightly declines with time under phase fluctuations. Therefore, the investigation of quantum features without considering quantum decoherences is just an assumption far from participial reality. The quantum scheme would probably be one of the best optical devices to simultaneously support steerable states, entangled state, and discordant state-based quantum information processing.

Appendix

Stochastic Differential Equations

In this Appendix, applying the master equation, we seek to derive the stochastic differential equations and the solutions of the cavity mode variables, which are important tool in studying the quantum properties of light. The c-number stochastic differential equations, which can be defined as the time evolution of the first and second moments of the cavity mode variables associated with the normal ordering, are mathematically easier to handle than the corresponding operator equations. Applying Equation (10) and the fact (Equation (A.1)), as well as considering the cyclic property of the trace operation and bosonic commutation relation, the time evolution of expectation value of the cavity mode variable can be found as

$$\frac{d}{dt}\langle \widehat{A}\rangle = Tr\left(\frac{d\widehat{\rho}(t)}{dt}\widehat{A}\right). \tag{A.1}$$

The time evolution of the expectation value of the cavity mode variables applying the cyclic property of the trace operation and taking into account the bosonic commutation relation turns out to be

$$\frac{d}{dt}\langle o_1\rangle = -\frac{\gamma_1}{2}\langle o_1\rangle + \frac{\nu_1}{2}\langle o_2^\dagger\rangle, \tag{A.2}$$

$$\frac{d}{dt}\langle \widehat{o}_2\rangle = -\frac{\gamma_2}{2}\langle \widehat{o}_2\rangle - \frac{\nu_2}{2}\langle \widehat{o}_1^\dagger\rangle, \tag{A.3}$$

$$\frac{d}{dt}\langle \widehat{o}_1^2\rangle = -\gamma_1\langle \widehat{o}_1^2\rangle + \nu_1\langle \widehat{o}_2^\dagger\widehat{o}_1\rangle, \tag{A.4}$$

$$\frac{d}{dt}\langle \widehat{o}_2^2\rangle = -\mu_2\langle \widehat{o}_2^2\rangle - \nu_2\langle \widehat{o}_1^\dagger\widehat{o}_2\rangle, \tag{A.5}$$

$$\frac{d}{dt}\langle \widehat{o}_1^\dagger\widehat{o}_1\rangle = -\gamma_1\langle \widehat{o}_1^\dagger\widehat{o}_1\rangle + \frac{\nu_1}{2}\left[\langle \widehat{o}_1^\dagger\widehat{o}_2^\dagger\rangle + \langle \widehat{o}_1\widehat{o}_2\rangle\right] + 2\Sigma_1 + \kappa\bar{N}_{th}, \tag{A.6}$$

$$\frac{d}{dt}\langle \widehat{o}_2^\dagger\widehat{o}_2\rangle = -\gamma_1\langle \widehat{o}_2^\dagger\widehat{o}_2\rangle - \frac{\nu_2}{2}\left[\langle \widehat{o}_2^\dagger\widehat{o}_1^\dagger\rangle + \langle \widehat{o}_1\widehat{o}_2\rangle\right] + \kappa\bar{N}_{th}, \tag{A.7}$$

$$\frac{d}{dt}\langle \widehat{o}_1^\dagger\widehat{o}_2\rangle = -\frac{1}{2}(\gamma_1+\gamma_2)\langle \widehat{o}_1^\dagger\widehat{o}_2\rangle - \frac{\nu_2}{2}\langle \widehat{o}_1^{\dagger 2}\rangle + \frac{\nu_1}{2}\langle \widehat{o}_2^2\rangle, \tag{A.8}$$

in which $\gamma_1 = \kappa - 2\Sigma_2$, $\gamma_2 = \kappa + 2\Sigma_2$, $\nu_1 = 2\Sigma_2$, and $\nu_2 = 2\Sigma_4$. Since the operators in Equations (A.2)-(A.8) are put in the normal order, they can be written in terms of the c-number equations associated to them as

$$\frac{d}{dt}\langle o_1\rangle = -\frac{\gamma_1}{2}\langle o_1\rangle + \frac{\nu_1}{2}\langle o_2^*\rangle, \tag{A.9}$$

$$\frac{d}{dt}\langle o_2\rangle = -\frac{\gamma_2}{2}\langle o_2\rangle - \frac{\nu_2}{2}\langle o_1^*\rangle, \tag{A.10}$$

$$\frac{d}{dt}\langle o_1^2\rangle = -\gamma_1\langle o_1^2\rangle + \nu_1\langle o_2^* o_1\rangle, \tag{A.11}$$

$$\frac{d}{dt}\langle o_2^2\rangle = -\gamma_2\langle o_2^2\rangle - \nu_2\langle o_1^* o_2\rangle, \tag{A.12}$$

$$\frac{d}{dt}\langle o_1^* o_1\rangle = -\gamma_1\langle o_1^* o_1\rangle + \frac{\nu_1}{2}\left[\langle o_1^* o_2^*\rangle + \langle o_1 o_2\rangle\right] + 2\Sigma_1 + \kappa\bar{N}_{th}, \tag{A.13}$$

$$\frac{d}{dt}\langle o_2^* o_2\rangle = -\gamma_2\langle o_2^* o_2\rangle - \frac{\nu_2}{2}\left[\langle o_2^* o_1^*\rangle + \langle o_1 o_2\rangle\right] + \kappa\bar{N}_{th}, \tag{A.14}$$

$$\frac{d}{dt}\langle o_1^* o_2\rangle = -\frac{1}{2}(\gamma_1+\gamma_2)\langle o_1^* o_2\rangle - \frac{\nu_2}{2}\langle o_1^{*2}\rangle + \frac{\nu_1}{2}\langle o_2^2\rangle, \tag{A.15}$$

$$\frac{d}{dt}\langle o_1^* o_2\rangle = -\frac{1}{2}(\gamma_1+\gamma_2)\langle o_1^* o_2\rangle - \frac{\nu_2}{2}\langle o_1^{*2}\rangle + \frac{\nu_1}{2}\langle o_2^2\rangle. \tag{A.16}$$

$$\langle o_1^*(t)o_1(t)\rangle = \left[\frac{(2\Sigma_1+\kappa\bar{N}_{th})(1-w)^2+\kappa\bar{N}_{th}y_+^2-(2\Sigma_4)y_+(1-w)}{8\lambda_+}\right]\left[1-e^{-2\lambda_+t}\right] + \left[\frac{(2\Sigma_1+\kappa\bar{N}_{th})(1+w)^2+\kappa\bar{N}_{th}y_+^2+(2\Sigma_4)y_+(1+w)}{8\lambda_-}\right]\left[1-e^{-2\lambda_-t}\right] + \left[\frac{(2\Sigma_1+\kappa\bar{N}_{th})(1-w^2)-\kappa\bar{N}_{th}y_+^2-(2\Sigma_4)y_+w}{2(\lambda_++\lambda_-)}\right]\left[1-e^{-(\lambda_++\lambda_-)t}\right], \tag{A.17}$$

$$\langle o_2^*(t)o_2(t)\rangle = \left[\frac{(2\Sigma_1+\kappa\bar{N}_{th})y_-^2+\kappa\bar{N}_{th}(1+w)^2-(2\Sigma_4)y_-(1+w)}{8\lambda_+}\right]\left[1-e^{-2\lambda_+t}\right] + \left[\frac{(2\Sigma_1+\kappa\bar{N}_{th})y_-^2+\kappa\bar{N}_{th}(1-w)^2+(2\Sigma_4)y_-(1-w)}{8\lambda_-}\right]\left[1-e^{-2\lambda_-t}\right] - \left[\frac{(2\Sigma_1+\kappa\bar{N}_{th})y_-^2-\kappa\bar{N}_{th}(1-w^2)-(2\Sigma_4)y_-w}{2(\lambda_++\lambda_-)}\right]\left[1-e^{-(\lambda_++\lambda_-)t}\right], \tag{A.18}$$

$$\langle o_1(t)o_2(t)\rangle = \langle o_1^*(t)o_2^*(t)\rangle, \tag{A.19}$$

$$\langle o_1^*(t)o_2(t)\rangle = 0. \tag{A.20}$$

Data Availability

The data used to support the findings of this study are included within the article.

Conflicts of Interest

The authors declare that there is no conflict of interest regarding the publication of this paper.

Acknowledgments

The authors acknowledge the support from the Jimma University, College of Natural Sciences, Research and Postgraduate Coordinating Office through a Mega Project Grant No. CNS-PHYS-14-2022/21.

References

[1] R. F. Werner, "Quantum states with Einstein-Podolsky-Rosen correlations admitting a hidden-variable model," *Physical Review A*, vol. 40, no. 8, pp. 4277–4281, 1989.

[2] C. H. Bennett and D. P. DiVincenzo, "Quantum information and computation," *Nature*, vol. 404, no. 6775, pp. 247–255, 2000.

[3] G. Benenti, G. Casati, D. Rossini, and G. Strini, *Principles of Quantum Computation and Information*, World Scientific Publishing, 2019.

[4] A. Streltsov, G. Adesso, and M. B. Plenio, "Colloquium: quantum coherence as a resource," *Reviews of Modern Physics*, vol. 89, no. 4, article 041003, 2017.

[5] M. Erhard, M. Krenn, and A. Zeilinger, "Advances in high-dimensional quantum entanglement," *Nature Reviews Physics*, vol. 2, no. 7, pp. 365–381, 2020.

[6] F. Shahandeh, A. P. Lund, and T. C. Ralph, "Quantum correlations and global coherence in distributed quantum computing," *Physical Review A*, vol. 99, no. 5, article 052303, 2019.

[7] M. Cuzminschi and A. Isar, "Quantum entanglement and quantum steering of two bosonic modes in noisy environments," *Romanian Journal of Physics*, vol. 66, p. 112, 2021.

[8] B. Deveaud, A. Quattropani, and P. Schwendimann, *Quantum Coherence in Solid State Systems*, IOS Press, 2009.

[9] Z. Alessandro, J. Fiurášek, and M. Bellini, "A high-fidelity noiseless amplifier for quantum light states," *Nature Photonics*, vol. 5, no. 1, pp. 52–56, 2011.

[10] X. Zhan, "Determining the mixed high-dimensional Bell state of a photon pair through the measurement of a single photon," *Physical Review A*, vol. 103, no. 3, article 032437, 2021.

[11] S. Mahmoodian, M. Čepulkovskis, S. Das, P. Lodahl, K. Hammerer, and A. S. Sørensen, "Strongly correlated photon transport in waveguide quantum electrodynamics with weakly coupled emitters," *Physical Review Letters*, vol. 121, no. 14, article 143601, 2018.

[12] S. Tesfa, *Quantum Optical Processes: From Basics to Applications*, Springer Nature, 2020.

[13] C. G. Feyisa, T. Abebe, T. Tessema et al., "Strongly-entangled twin beams produced by a coherent beat laser coupled to thermal reservoir," *Journal of Russian Laser Research*, vol. 42, no. 1, pp. 1–19, 2021.

[14] S. Ullah, H. S. Qureshi, and F. Ghafoor, "Hierarchy of temporal quantum correlations using a correlated spontaneous emission laser," *Optics Express*, vol. 27, no. 19, pp. 26858–26873, 2019.

[15] M. O. Scully and M. S. Zubairy, "Theory of the quantum-beat laser," *Physical Review A*, vol. 35, no. 2, pp. 752–758, 1987.

[16] J. Liu, R. Su, Y. Wei et al., "A solid-state source of strongly entangled photon pairs with high brightness and indistinguishability," *Nature Nanotechnology*, vol. 14, no. 6, pp. 586–593, 2019.

[17] H. S. Qureshi, S. Ullah, and F. Ghafoor, "Generation and control of bipartite entanglement in a correlated spontaneous-emission laser," *Journal of Russian Laser Research*, vol. 42, no. 5, pp. 501–511, 2021.

[18] R. Uola, A. C. Costa, H. C. Nguyen, and O. Gühne, "Quantum steering," *Reviews of Modern Physics*, vol. 92, no. 1, article 015001, 2020.

[19] W. H. Louisell, *Quantum Statistical Properties of Radiation*, Wiley, New York, NY, USA, 1973.

[20] E. A. Sete, "Effect of dephasing on transient and steady-state entanglement in a quantum- beat laser," *Physical Review A*, vol. 84, no. 6, article 063808, 2011.

[21] G. S. Agarwal, "Quantum statistical theories of spontaneous emission and their relation to other approaches," in *Springer Tracts in Modern Physics*, pp. 1–128, 1974.

[22] I. Kogias, R. A. Lee, S. Ragy, and G. Adesso, "Quantification of Gaussian quantum steering," *Physical Review Letters*, vol. 114, no. 6, article 060403, 2015.

[23] H. M. Wiseman, S. J. Jones, and A. C. Doherty, "Steering, entanglement, nonlocality, and the Einstein-Podolsky-Rosen paradox," *Physical Review Letters*, vol. 98, no. 14, article 140402, 2007.

[24] L. M. Duan, G. Giedke, J. I. Cirac, and P. Zoller, "Entanglement purification of Gaussian continuous variable quantum states," *Physical Review Letters*, vol. 84, no. 17, pp. 4002–4005, 2000.

[25] D. Luong, S. Rajan, and B. Balaji, "Entanglement-based quantum radar: from myth to reality," *IEEE Aerospace and Electronic Systems Magazine*, vol. 35, no. 4, pp. 22–35, 2020.

[26] K. Umemoto, "Quantum and classical correlations inside the entanglement wedge," *Physical Review D*, vol. 100, no. 12, article 126021, 2019.

[27] C. Gupta, "Optimization of modified quantum discord in projector space," *Brazilian Journal of Physics*, vol. 51, no. 5, pp. 1466–1471, 2021.

[28] O. Jeff, *Quantum Optics for Experimentalists*, World Scientific, 2017.

[29] H. Goto, H. Katsuki, H. Ibrahim, H. Chiba, and K. Ohmori, "Strong-laser-induced quantum interference," *Nature Physics*, vol. 7, no. 5, pp. 383–385, 2011.

[30] C. Gashu and T. Abebe, "Externally induced entanglement amplification in a coherently pumped emission of laser with parametric amplifier and coupled to squeezed vacuum reservoir," *Physica Scripta*, vol. 95, no. 7, article 075105, 2020.

[31] Q. Y. He, Q. H. Gong, and M. D. Reid, "Classifying directional Gaussian entanglement, Einstein-Podolsky-Rosen steering, and discord," *Physical Review Letters*, vol. 114, no. 6, article 060402, 2015.